



# Refractive Index Sensor Based on Surface Plasmon Resonance Excitation in a D-Shaped Photonic Crystal Fiber Coated by Titanium Nitride

Yashar Esfahani Monfared<sup>1,2</sup>

Received: 17 July 2019 / Accepted: 3 November 2019 / Published online: 22 November 2019  
© Springer Science+Business Media, LLC, part of Springer Nature 2019

## Abstract

In this paper, a plasmonic refractive index sensor using a D-shaped photonic crystal fiber coated by titanium nitride has been proposed. The interaction and interplay between fiber fundamental mode and plasmonic mode which lead to the formation of resonance peaks depending on the analyte refractive index (RI) are explained in detail. Using both spectral and amplitude sensitivity methods, the sensing performance of the proposed sensor for detecting high-index analytes is numerically investigated. The proposed PCF-SPR sensor has a RI detection range of 1.44 to 1.52 and exhibits two linear sensing regions with an average spectral sensitivity of  $-16,275$  nm/RIU for analyte RI ranging from 1.44 to 1.48, and  $-7571$  nm/RIU for analyte RI between 1.485 and 1.52, respectively. We also study the amplitude sensitivity of the proposed sensor which shows promising value of  $206.25$  RIU<sup>-1</sup> for 1650-nm excitation. The proposed RI sensor is an attractive platform for detecting various high RI chemical and biochemical samples due to simple design, cost-effective plasmonic material, relatively large detection range, high sensitivity, and promising linear sensing performance.

**Keywords** Photonic crystal fiber sensor · Plasmonic sensor · Titanium nitride · Plasmonic materials

## Introduction

Plasmonics examines the interaction between electromagnetic waves and surface electrons at the interface between metals and dielectrics [1]. As a rapidly developing field, plasmonics has opened the door to a wide range of interesting applications including medical diagnostics via surface enhanced Raman spectroscopy [2], subwavelength communication devices [3], and highly sensitive sensors and biosensors [4]. Surface plasmon resonance (SPR) refers to the excitation of surface plasmons (SPs) which are collective and coherent oscillation of the surface electrons due to the incident electromagnetic field [1]. Excitation of SPs is usually accompanied by a strong absorption or scattering of the incident electromagnetic field. As this absorption/scattering is strongly dependent on the refractive index (RI) of the surrounding medium at the

dielectric/metal interface, RI sensing is possible by monitoring the variations in the loss peak [4]. Between different plasmonic sensors, photonic crystal fiber-based surface plasmon resonance (PCF-SPR) sensors are the most promising candidates to satisfy the small probe size as well as ultrahigh sensitivity requirements in biological, environmental, and medical applications [4, 5].

The most common plasmonic materials used in the previous reported PCF-SPR sensors are gold and silver because of their optical properties and chemical stability [6]. However, the relatively high cost of these metals is a major drawback to the mass manufacture of the plasmonic devices with gold or silver films. Furthermore, gold and silver can soften at relatively low temperatures which can cause a complete loss of the ability of material to excite SPs [6]. Therefore, an ideal alternative plasmonic material should offer lower production cost, higher melting point, lower intrinsic loss, compatibility with standard nanofabrication processes, and tunability [6, 7].

In a quest to find alternative plasmonic materials, researchers paid a great amount of attention to semiconductors, transparent conducting oxides (TCOs), cheap metals, and inter-metallics [6, 7]. To this end, PCF-SPR sensors based on hybrid plasmonic materials such as copper/graphene [8], graphene/gold, or graphene/silver [9] have been reported.

✉ Yashar Esfahani Monfared  
y.monfared@dal.ca

<sup>1</sup> Department of Physics and Atmospheric Science, Dalhousie University, Halifax, NS, Canada

<sup>2</sup> Department of Chemistry, Dalhousie University, Halifax, NS, Canada

Recently, titanium nitride (TiN)-coated [10] and titanium-assisted [11] PCF-SPR biosensors with complex structure and different airhole diameters have been studied. Between these alternative materials, refractory metals have high melting point and excellent chemical stability. Among different refractory metals, TiN has already received great attention and has been considered as a promising candidate for plasmonic applications at optical frequencies and at high temperatures [12]. TiN has a very high melting point and high chemical stability at temperatures above 2000°C. TiN also has high conductivity, CMOS compatibility, and corrosion resistance which makes it an ideal material for plasmonic applications [10, 12].

In this paper, we investigate the deposition of TiN nanofilm on a simple D-shaped PCF and study the RI sensing performance of the sensor in detail. To the best of our knowledge, this is the first time that TiN nanofilms are being investigated in a PCF-SPR biosensor with simple (single airhole size) D-shaped structure for detecting high-index analytes. Simple single-airhole-size D-shaped PCF-SPR sensors offer numerous advantages including ease of fabrication [13, 14], compatibility with existing optical communication systems, compact size, and ultra-large sensitivity [13, 14]. We demonstrate the superior characteristics of our proposed sensor to detect analytes with RI between 1.44 and 1.52. We will also study the effect of design parameters and any fabrication-induced imperfections on the performance of the proposed sensor.

## Sensor Design

We design our PCF-SPR sensor with a simple and well-established quasi-D-shaped structure with single airhole dimension. Our PCF-SPR sensor has four design parameters overall: airhole diameter ( $d_{\text{holes}}$ ), core diameter ( $d_{\text{core}}$ ), center-to-center spacing between holes ( $A$ ) and TiN layer thickness ( $t_{\text{TiN}}$ ). The cross section of our proposed PCF-SPR sensor with all of the design parameters and materials is shown in Fig. 1.

To design the biosensor, we use silica as the cladding material, the liquid analyte as the filling material in the hollow-core which is surrounded by period array of airholes and TiN nanofilm deposition on top of the structure as the plasmonic material. To accurately simulate the structure, we took the material dispersion of silica and TiN into account. Wavelength-dependent RI of silica can be calculated using the following Sellmeier's formula [15, 16]:

$$n_{\text{silica}}^2(\lambda) = 1 + \frac{0.6961663\lambda^2}{\lambda^2 - 0.0684043^2} + \frac{0.4079426\lambda^2}{\lambda^2 - 0.1162414^2} + \frac{0.8974794\lambda^2}{\lambda^2 - 9.896161^2}, \quad (1)$$

where  $\lambda$  is the excitation wavelength in micrometer. The wavelength-dependent complex RI of TiN has a form of

$$n_{\text{TiN}}(\lambda) = n(\lambda) + ik(\lambda), \quad (2)$$

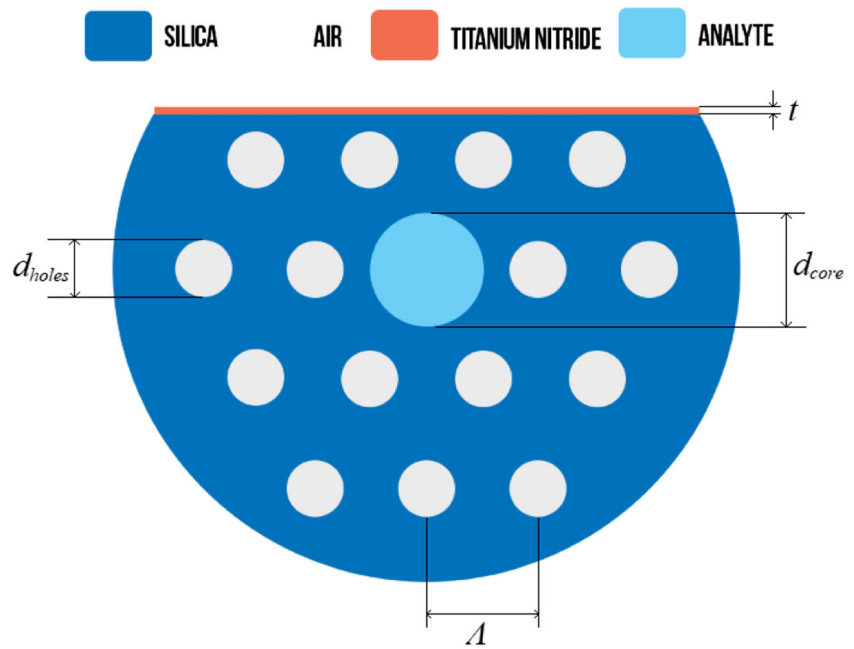
where  $n(\lambda)$  is the real part of the RI and  $k(\lambda)$  is the imaginary part of the RI which is called extinction coefficient. In Fig. 2, we plot the complex RI of TiN, including real part of the RI and imaginary part of the RI, as a function of excitation wavelength according to the model presented in [17, 18]. The analyte refractive index variation is between 1.44 and 1.52 in our simulations. We used a finite element method (FEM) and perfectly matched layers (PML) boundary condition applied with Comsol Multiphysics software to simulate fiber modes and plasmonic modes. To further minimize the computational errors and ensure the accuracy of the results, an extra-fine mesh size (minimum element size of 5 nm and maximum element size of 500 nm) has been utilized. We also performed rigorous convergence analysis (error threshold of  $10^{-5}$ ) and manually checked the solutions to make sure every solution meets our error criteria. The results for fundamental mode of the fiber have been compared with finite difference time domain (FDTD) simulations using OptiFDTD software, and similar mode indices have been obtained. Finally, RI calculations, modes, and the resulting data have been analyzed in MATLAB R2015b.

## Results and Discussions

### Mechanism

The sensing mechanism in our proposed D-shaped sensor is based on the coupling between plasmonic mode (TiN nanofilm) and fundamental guiding mode of the PCF (analyte-guided mode). We now demonstrate the excitation of these modes in our PCF-SPR sensor where excitation wavelength is 1550 nm,  $d_{\text{holes}}/A = 0.16$ ,  $d_{\text{core}}/A = 0.66$ ,  $A = 6 \mu\text{m}$ , and  $t_{\text{TiN}} = 50 \text{ nm}$ . There is no guiding mode in the hollow-core of the PCF when there is no analyte. By filling the core of the PCF with a high-index analyte, the guiding mode will appear. By increasing the analyte RI from 1.45 to 1.52, the effective area of the fundamental guiding mode reduces significantly. This reduced effective area will lead to less effective surface plasmon excitation, resulting in a weak coupling between fiber mode and plasmonic mode. If we further increase the analyte RI by values larger than 1.52, the fiber mode will not couple to plasmon mode anymore and the structure cannot be used as a sensor. We also observed multi-mode operation for analyte RI larger than 1.48 and single mode operation for analyte RI between 1.44 and 1.48 which can contribute directly to efficient surface plasmon excitation at this RI range.

**Fig. 1** The cross section of the proposed PCF-SPR sensor with different design parameters: air-holes diameter ( $d_{holes}$ ), core diameter ( $d_{core}$ ), holes pitch ( $A$ ), and titanium nitride layer thickness ( $t$ )



During our simulations, we note that the coupling is much stronger in the case of y-polarized light (see the y-axis in Fig. 3), and therefore, we only studied this case in our investigations.

In order to understand underlying coupling mechanism between fiber mode and plasmonic mode, we tracked the variations in the effective index ( $n_{eff}$ ) of fiber fundamental mode and plasmonic mode inside the PCF-SPR structure. As seen in Fig. 4, by changing the excitation wavelength,  $n_{eff}$  of fiber mode and plasmonic decreases with different rates. As a result, there is a specific wavelength in which these two values

( $n_{eff-fiber}$  and  $n_{eff-plasmonic}$ ) are both equal to each other. At this point, we have the maximum coupling between fiber mode and plasmonic mode which can in turn result in a peak in confinement loss spectra of the guiding mode. Confinement loss is directly related to imaginary part of  $n_{eff}$  and can be calculated from [19].

$$\alpha \text{ (dB/cm)} = \frac{8.686 \times 2\pi \times \text{Im}(n_{eff}) \times 10^7}{\lambda}, \tag{3}$$

where  $\lambda$  is excitation wavelength in nanometer. This excitation wavelength which results in a maximum confinement loss is called resonance wavelength ( $\lambda_{resonance}$ ) of the structure, which is strongly dependent on the PCF-SPR design parameters and particularly, analyte RI. Therefore, by tracking changes in resonance wavelength of the structure, we can easily detect an unknown analyte in the PCF core.

In order to further realize the effect of analyte RI on the confinement loss spectra of the sensor, we simulate the real and imaginary part of the effective mode index of the fiber fundamental mode and plasmonic mode when analyte RI is 1.47. As seen in Fig. 5, real parts of the effective mode index of the fiber mode and plasmonic mode are both equal to each other around 1235 nm. We can clearly see that increasing the analyte RI from 1.45 in Fig. 4 to 1.47 in Fig. 5 causes a blueshift of resonance peak from around 1640 to 1235 nm.

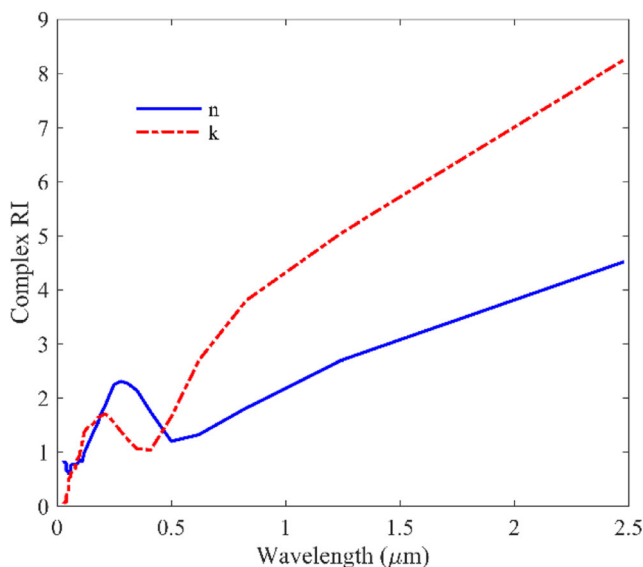
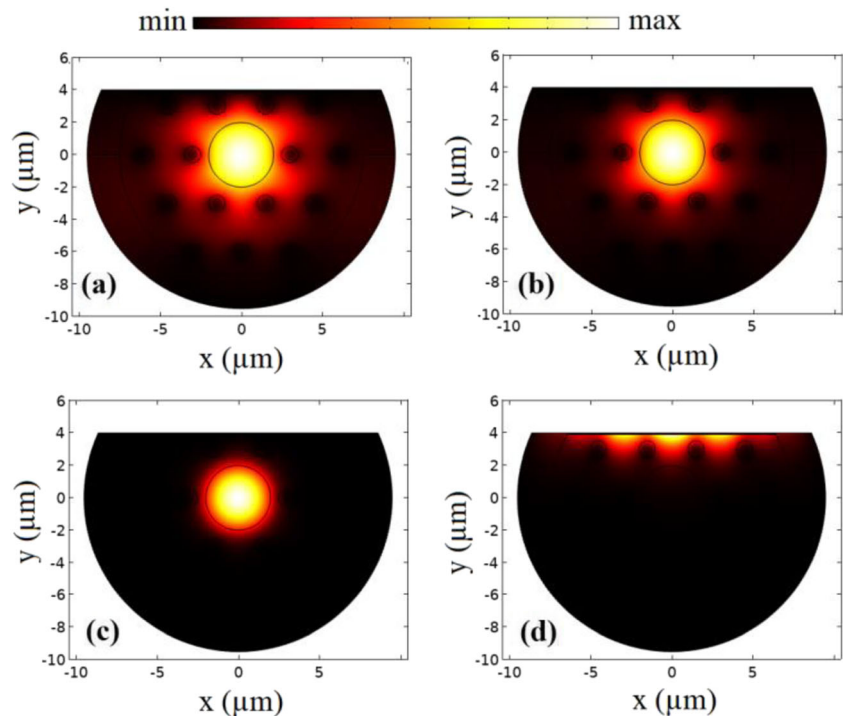


**Fig. 2** Complex refractive index of TiN as a function of excitation wavelength. The solid blue curve is the real part of the refractive index, and the red dash-dotted curve represent imaginary part of refractive index or extinction coefficient

### The Role of Design Parameters

We first analyze the impact of the design parameters of the proposed sensor on the location of the  $\lambda_{resonance}$  or maximum point of loss spectra. As seen in Fig. 6, the resonance

**Fig. 3** The electric field distribution of the proposed PCF-SPR sensor at 1550 nm for **a** fiber fundamental guiding mode with analyte RI of 1.45, **b** fiber fundamental guiding mode with analyte RI of 1.48, **c** fiber fundamental guiding mode with analyte RI of 1.52, and **d** plasmonic mode for analyte RI of 1.45. Note that the design parameters are  $d_{\text{holes}}/\Lambda = 0.16$ ,  $d_{\text{core}}/\Lambda = 0.66$ ,  $\Lambda = 6 \mu\text{m}$ , and  $t_{\text{TiN}} = 50 \text{ nm}$



wavelength of the structure depends on the design parameters of the PCF-SPR sensor including TiN layer thickness ( $t$ ), air-hole diameter ( $d_{\text{holes}}$ ), and core diameter ( $d_{\text{core}}$ ). As seen in Fig. 6a, by increasing  $t$  from 40 to 60 nm, the resonant wavelength blueshifts from approximately 1730 to 1580 nm. The same trend exists for  $d_{\text{core}}$  in Fig. 6c, where increasing core diameter ratio ( $d_{\text{core}}/\Lambda$ ) from 0.6 to 0.72 results in a resonance wavelength blueshift from 1686 to 1592 nm. However, as

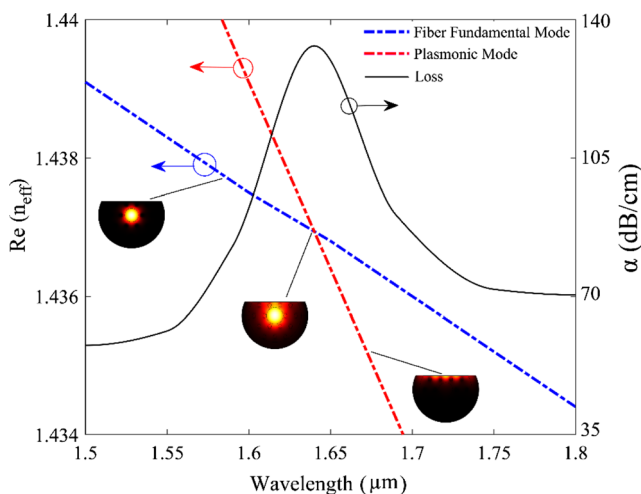


**Fig. 4** Real part of effective index of fiber core fundamental mode ( $n_{\text{eff-fiber}}$ ) and plasmonic mode ( $n_{\text{eff-plasmonic}}$ ) as a function of wavelength. The design parameters are  $d_{\text{holes}}/\Lambda = 0.16$ ,  $d_{\text{core}}/\Lambda = 0.66$ ,  $\Lambda = 6 \mu\text{m}$ , and  $t_{\text{TiN}} = 50 \text{ nm}$ ; analyte RI is 1.45. The resonance peak (peak of confinement loss) appears where the real part of effective index of fiber mode and plasmonic mode matches ( $n_{\text{eff-fiber}} = n_{\text{eff-plasmonic}}$ ). Insets show electric field distribution at different points in spectra for fiber mode, plasmonic mode, and the coupled core-plasmonic mode at resonance wavelength

seen in Fig. 6b, an increase in airhole diameter ratio will result in a resonant wavelength redshift from 1595 to 1681 nm. According to our extensive simulations, these are the optimized ranges of variation for design parameters of the PCF-SPR sensor as the most effective mode coupling between the fiber and plasmonic modes can happen at these values.

Next, we fix the design parameters at  $d_{\text{holes}}/\Lambda = 0.16$ ,  $d_{\text{core}}/\Lambda = 0.66$ ,  $\Lambda = 6 \mu\text{m}$ , and  $t_{\text{TiN}} = 50 \text{ nm}$  and focus on analyzing the performance of the proposed biosensor. We analyzed both spectral sensitivity and amplitude sensitivity of the sensor where analyte RI changing from 1.44 to 1.52.

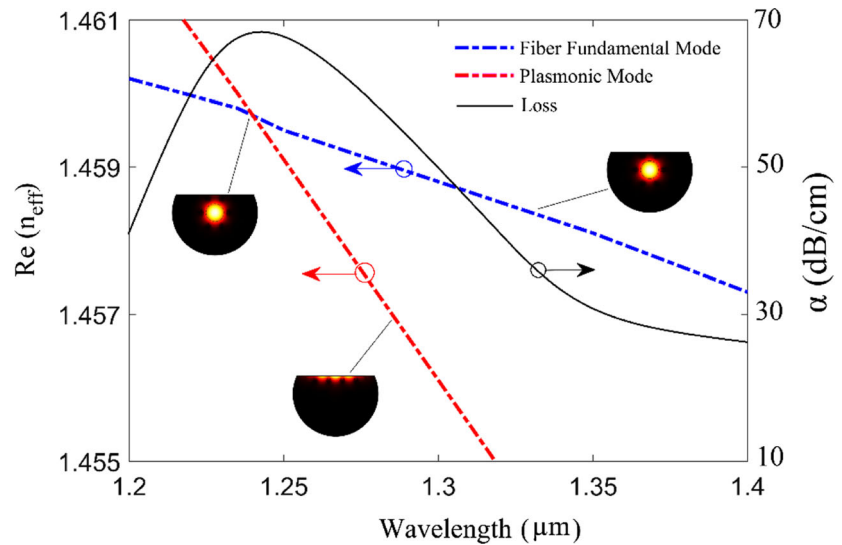
### Spectral Sensitivity

By measuring the amount of shift in the resonance peak ( $\Delta\lambda_{\text{resonance}}$ ) due to a change in the analyte RI ( $\Delta n_{\text{analyte}}$ ), the spectral sensitivity of the sensor can be determined in RI units (RIU) as [20].

$$\text{Ssp}(\text{nm}/\text{RIU}) = \frac{\Delta\lambda_{\text{resonance}}}{\Delta n_{\text{analyte}}}, \quad (4)$$

Here, we study analyte RI ranging from 1.44 to 1.52. For analyte RI smaller than 1.44 and larger than 1.52, the sensitivity is not enough to detect a small change in RI. For any analyte RI higher than 1.52, most of the laser energy will be confined in the PCF core which leads to a weak coupling between plasmonic mode and fiber mode and therefore a low sensitivity. Therefore, the range of operation of our

**Fig. 5** Real part of effective index of fiber core fundamental mode ( $n_{\text{eff-fiber}}$ ) and plasmonic mode ( $n_{\text{eff-plasmonic}}$ ) as a function of wavelength. The design parameters are  $d_{\text{holes}}/\Lambda = 0.16$ ,  $d_{\text{core}}/\Lambda = 0.66$ ,  $\Lambda = 6 \mu\text{m}$ , and  $t_{\text{TiN}} = 50 \text{ nm}$ ; analyte RI is 1.47. The insets show electric field distribution at different points in spectra for fiber mode, plasmonic mode, and the coupled core-plasmonic mode at resonance wavelength



plasmonic biosensor is 1.44 to 1.52 (0.8 RIU). In Fig. 6, we analyzed the sensitivity of the proposed PCF-SPR refractometer with the analyte RI ranging from 1.44 to 1.52.

According to Fig. 7, the resonance peak location and sensitivity of the PCF-SPR sensor strongly depend on the analyte RI. Based on the sensitivity, we can divide the performance of our sensor into two linear sensing regions. The first region is for analyte RI ranging from 1.44 to 1.48 which shows a promising linear behavior (coefficient of determination for linear fit is 0.998) with an ultrahigh average linear sensitivity of  $-16,275 \text{ nm/RIU}$ . The second region is for analyte RI ranging from 1.485 to 1.52 which shows an average linear sensitivity of  $-7571 \text{ nm/RIU}$ . The sensitivity outside this RI range decays exponentially to zero, and therefore, the sensor is only appropriate for sensing analyte with RI ranging from 1.44 to 1.52. As seen in Fig. 7, by increasing analyte RI, the resonance peak blueshifts significantly. The blueshift of resonance wavelength by increasing analyte RI is an interesting behavior of analyte-filled PCF-SPR sensors which directly contradicts the behavior of other PCF-SPR sensors in which the resonance wavelength redshifts by increasing analyte RI [20, 21]. The reason for this contradiction is the way we fill the analyte into PCF-SPR sensor [22]. The analyte is filled into airholes or

channels in most of the PCF-SPR designs [19, 23] whereas here we filled the analyte directly into the PCF core. This is also why we can sense a wide range of high-index analyte liquids. In airhole-filled or channel-filled PCF-SPR sensors, the analyte RI should be lower than that of the silica (1.44) to keep the total internal reflection guiding mechanism of the fiber. As we fill the core of our fiber with analyte, we are not limited to 1.44 as the upper limit of RI detection.

### Amplitude Sensitivity

By measuring the loss of optical power at a fixed wavelength ( $\Delta\alpha$ ) due to a change in analyte RI ( $\Delta n_{\text{analyte}}$ ), the amplitude sensitivity of the PCF-SPR sensor can be determined as [20]

$$Sa \text{ (RIU}^{-1}\text{)} = \frac{\Delta\alpha(\lambda, n_{\text{analyte}})/\Delta n_{\text{analyte}}}{\alpha(\lambda, n_{\text{analyte}})} \tag{5}$$

where  $\alpha(\lambda, n_{\text{analyte}})$  is the fiber mode confinement loss at a particular wavelength and RI. The sensitivity and range of detection are usually higher in the case of spectral method, but the main advantage of amplitude method is reduced costs

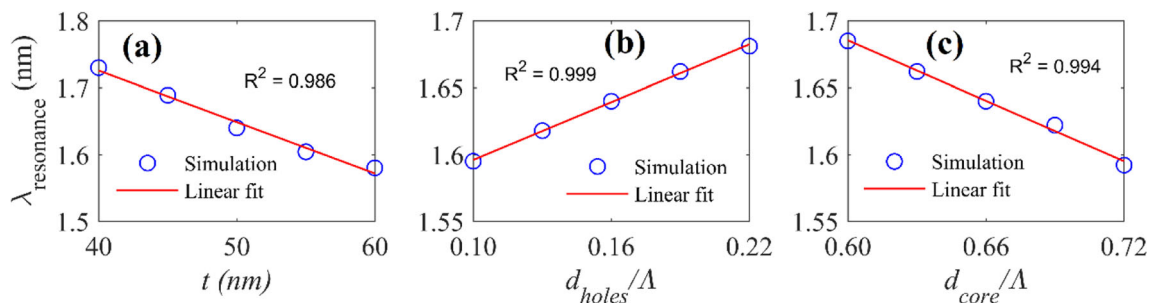
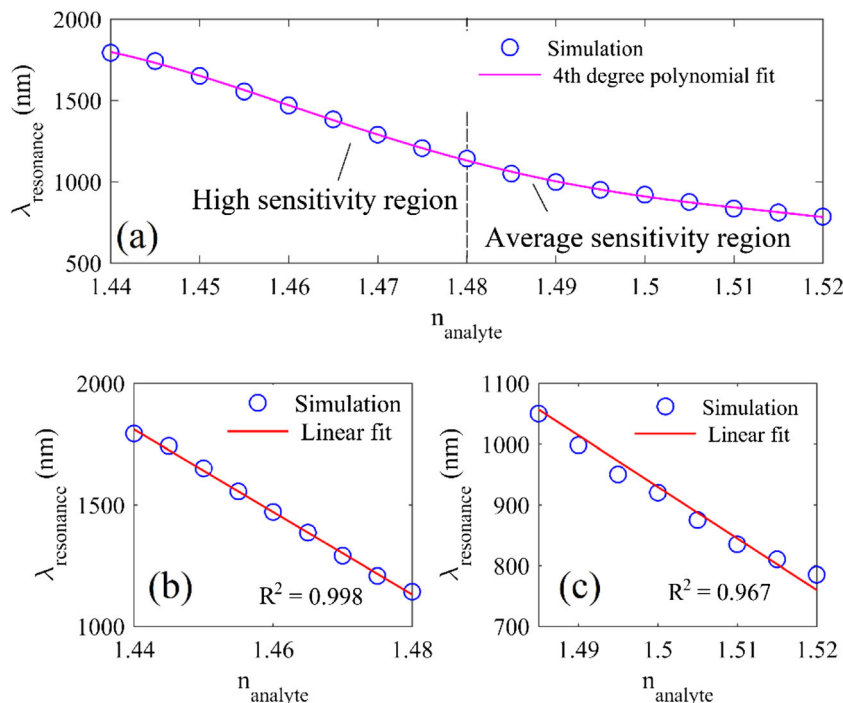


**Fig. 6** Resonance wavelength location as a function of **a** TiN layer thickness where  $d_{\text{holes}}/\Lambda = 0.16$ ,  $d_{\text{core}}/\Lambda = 0.66$ , and  $\Lambda = 6 \mu\text{m}$ ; **b** airholes diameter ratio where  $d_{\text{core}}/\Lambda = 0.66$ ,  $\Lambda = 6 \mu\text{m}$ , and  $t_{\text{TiN}} = 50 \text{ nm}$ ; and **c**

core diameter ratio where  $d_{\text{holes}}/\Lambda = 0.16$ ,  $\Lambda = 6 \mu\text{m}$ , and  $t_{\text{TiN}} = 50 \text{ nm}$ . Analyte RI is fixed at 1.45 in all simulations



**Fig. 7** Resonance wavelength location as a function of **a** analyte RI from 1.44 to 1.52 where there are two sensing regions based on the sensitivity and linearity, **b** analyte RI from 1.44 to 1.48 in the high sensitivity region, and **c** analyte RI from 1.485 to 1.52 in the average sensitivity region. The sensor parameters are  $d_{\text{holes}}/\Lambda = 0.16$ ,  $d_{\text{core}}/\Lambda = 0.66$ ,  $\Lambda = 6 \mu\text{m}$ , and  $t_{\text{TiN}} = 50 \text{ nm}$



for the experiment. The method is cost-efficient because we simply do not need the spectral detection and adjustable laser sources which can be expensive depending on the setup. For example, we can only utilize a commercially available single wavelength low-cost laser and measure the amount of loss for different analyte RIs and detect an unknown analyte. The operation range and sensitivity strongly depend on the excitation wavelength of the laser source. In Fig. 8, we analyzed the amplitude sensitivity of the proposed sensor in vicinity of analyte RI of 1.45 with 1550- and 1650-nm excitations.

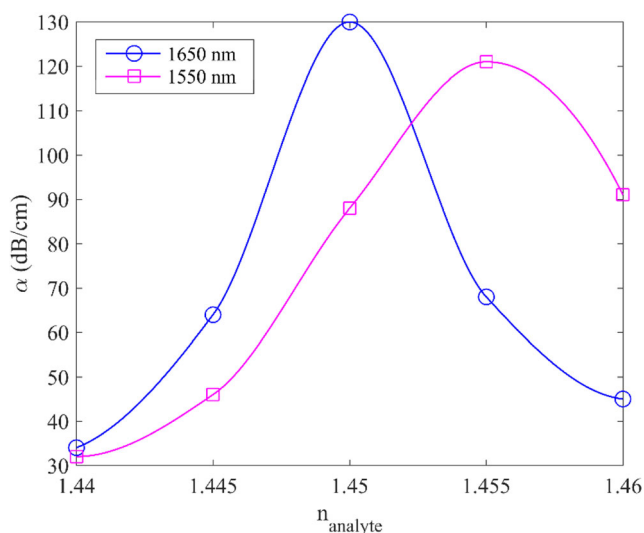


**Fig. 8** Confinement loss of the proposed PCF-SPR sensor as a function of analyte RI in two different excitation wavelengths. The sensor parameters are  $d_{\text{holes}}/\Lambda = 0.16$ ,  $d_{\text{core}}/\Lambda = 0.66$ ,  $\Lambda = 6 \mu\text{m}$ , and  $t_{\text{TiN}} = 50 \text{ nm}$

As seen in Fig. 8, the amplitude sensitivity can vary significantly with respect to different excitation wavelengths and analyte RIs. The detection range is also limited compared with the spectral method as loss variations are only significant close to the resonance wavelength. The amplitude sensitivities of the proposed biosensor are  $206.25 \text{ RIU}^{-1}$  with a 1650-nm excitation close to analyte RI of 1.45, and  $72.72 \text{ RIU}^{-1}$  with 1550-nm excitation close to analyte RI of 1.455. Using the sensitivity value and the full width at half maximum (FWHM) bandwidth of the confinement loss spectra of our sensor, we can calculate the figure of merit (FOM) [19] of the proposed biosensor as

$$\text{FOM} = \frac{S \text{ (nm/RIU)}}{\text{FWHM (nm)}}, \tag{6}$$

Using Eq. 6, we calculated the average FOM of our sensor in high sensitivity region for analyte RI between 1.44 and 1.48 (maximum FOM) to compare the performance of our sensor to other similarly reported PCF-SPR biosensors in the literature. We also calculate the average FOM of our sensor for analyte RI between 1.44 and 1.52 which is equal to 21. In Table 1, the simplicity of the design, detection range, sensitivity, and maximum FOM of our proposed sensor are compared to some of the previously reported high-index PCF-SPR sensors based on gold as the plasmonic material [19, 20, 23]. As we can clearly see in Table 1, the proposed TiN biosensor has a relatively broad detection range, simple design, and high sensitivities compare with the gold-based high-index PCF-SPR sensors which make it an attractive device for the

**Table 1** Comparison of the design and performance of the recent proposed PCF-SPR biosensors for high-index analyte detection

Properties	Ref [19]	Ref [20]	Ref [23]	This work
Plasmonic material	Gold	Gold	Gold	TiN
Sensor design	Channel-filled	D-shaped	Channel-filled	Simple D-shaped
Detection range	1.44–1.57	1.43–1.48	1.46–1.52	1.44–1.52
Max $S_{sp}$	4400 nm/RIU	7200 nm/RIU	6100 nm/RIU	– 16,275 nm/RIU
Max $S_a$	–	91 RIU <sup>-1</sup>	–	206.25 RIU <sup>-1</sup>
Max FOM	62.2 /RIU	–	–	147.9/RIU

detection of chemical and biochemical samples in different applications.

## Conclusion

A simple D-shaped photonic crystal fiber coated with titanium nitride is proposed as a plasmonic refractive index sensor. The sensor can detect high refractive index (RI) liquid analytes with a detection range of 0.8 RIU, ranging from 1.44 to 1.52. Using spectral and amplitude sensitivity methods, the resonance wavelength location and amount of confinement loss are numerically calculated. Our studies revealed that the proposed biosensor show two linear sensing regions with an average spectral sensitivity of – 16,275 nm/RIU for analyte RI ranging from 1.44 to 1.48, and – 7571 nm/RIU for analyte RI between 1.485 and 1.52, respectively. The amplitude sensitivities of the proposed sensor also exhibit promising value of 206.25 RIU<sup>-1</sup> for 1650-nm excitation. We also introduced a figure of merit and compare the performance of our sensor to similar RI sensors based on PCF. As our proposed RI sensor has a rather simple structure and it shows promising linear sensing performance, it can be an interesting platform for detecting various high RI chemical and biochemical samples in chemical, biological, and medical applications.

**Acknowledgments** Y. M. would like to thank Dalhousie University, Optiwave Corporation, and Killam Trusts for providing resources to perform this project. The author also thanks Amir Ahmadian for proofreading the final draft.

## References

- Stockman MI (2011) Nanoplasmonics: past, present, and glimpse into future. *Opt Express* 19:22029–22106
- Maier SA (2006) Plasmonic field enhancement and SERS in the effective mode volume picture. *Opt Express* 14:1957–1964
- Merlo JM et al (2016) Wireless communication system via nano-scale plasmonic antennas. *Sci Rep* 6:31710
- Liu C, Yang L, Lu X, Liu Q, Wang F, Lv J, Sun T, Mu H, Chu PK (2017) Mid-infrared surface plasmon resonance sensor based on photonic crystal fibers. *Opt Express* 25:14227–14237
- Khalek MA, Chakma S, Ahmed K, Paul BK, Vigneswaran D, Zakaria R (2018) Materials effect in sensing performance based on surface plasmon resonance using photonic crystal fiber. *Plasmonics*:1–7
- Naik GV, Shalae VM, Boltasseva A (2013) Alternative plasmonic materials: beyond gold and silver. *Adv Mater* 25:3264–3294
- Naik GV, Kim J, Boltasseva A (2011) Oxides and nitrides as alternative plasmonic materials in the optical range. *Opt Mater Express* 1:1090–1099
- Rifat AA et al (2016) Copper-graphene-based photonic crystal fiber plasmonic biosensor. *IEEE Photon J* 8(1):1–8
- Paul AK, Sarkar AK, Razzak SMA (2017) Graphene coated photonic crystal fiber biosensor based on surface plasmon resonance. *IEEE Region 10 Humanitarian Technology Conference, Dhaka, 856–859*
- Khalil AE, El-Saeed AH, Ibrahim MA, Hashish ME, Abdelmonem MR, Hameed MF, Azab MY, Obayy SAS (2018) Highly sensitive photonic crystal fiber biosensor based on titanium nitride. *Opt Quan Electron* 50(3):128
- Jabin MA, Ahmed K, Rana MJ, Paul BK, Islam M, Vigneswaran D, Uddin MS (2019) Surface plasmon resonance based titanium coated biosensor for cancer cell detection. *IEEE Photon J* 11(4):1–10
- Naik GV, Schroeder JL, Ni X, Kildishev AV, Sands TD, Boltasseva A (2012) Titanium nitride as a plasmonic material for visible and near-infrared wavelengths. *Opt Mater Express* 2:478–489
- Wu T, Shao Y, Wang Y, Cao S, Cao W, Zhang F, Liao C, He J, Huang Y, Hou M, Wang Y (2017) Surface plasmon resonance biosensor based on gold-coated side-polished hexagonal structure photonic crystal fiber. *Opt Express* 25:20313–20322
- Xie Q, Chen Y, Li X, Yin Z, Wang L, Geng Y, Hong X (2017) Characteristics of D-shaped photonic crystal fiber surface plasmon resonance sensors with different side-polished lengths. *Appl Opt* 56:1550–1555
- Monfared YE, Liang C, Khosravi R, Kacerovska B, Yang S (2019) Selectively toluene-filled photonic crystal fiber Sagnac interferometer for temperature sensing applications. *Results in Physics* 13: 102297
- Monfared YE, Ponomarenko SA (2019) Extremely nonlinear carbon-disulfide-filled photonic crystal fiber with controllable dispersion. *Opt Material* 88:406–411
- Pflüger J, Fink J, Weber W, Bohnen KP, Crecelius G (1984) Dielectric properties of TiCx, TiNx, VCx, and VNx from 1.5 to 40 eV determined by electron-energy-loss spectroscopy. *Phys Rev B* 30:1155–1163
- Dai M et al (2019) Measurement of optical constants of TiN and TiN/Ti/TiN multilayer films for microwave kinetic inductance photon-number-resolving detectors. *J Low Temp Phys* 194(5–6): 361–369
- Chu S, Nakkeeran K, Abobaker AM, Aphale SS, Babu PR, Senthilnathan K (2019) Design and analysis of surface-plasmon-resonance-based photonic quasi-crystal Fiber biosensor for high-refractive-index liquid analytes. *IEEE J Sel Top Quant* 25(2):1–9
- Luan N, Zhao L, Lian Y, Lou S (2018) A high refractive index plasmonic sensor based on D-shaped photonic crystal fiber with laterally accessible hollow-Core. *IEEE Photon J* 10(5):1–7

21. Hossen MN, Ferdous M, Khalek MA, Chakma S, Paul BK, Ahmed K (2018) Design and analysis of biosensor based on surface plasmon resonance. *Sensing and Bio-Sensing Research* 21:1–6
22. Shuai B, Xia L, Liu D (2012) Coexistence of positive and negative refractive index sensitivity in the liquid-core photonic crystal fiber based plasmonic sensor. *Opt Express* 20:25858–25866
23. Chu S, Nakkeeran K, Abobaker AM, Aphale SS, Babu PR, Senthilnathan K (2018) A surface plasmon resonance based photonic quasi-crystal fibre biosensor with fan-shaped analyte channel for high refractive index analytes. 2018 Conference on Lasers and Electro-Optics Pacific Rim (CLEO-PR), Hong Kong, 1–2

**Publisher's Note** Springer Nature remains neutral with regard to jurisdictional claims in published maps and institutional affiliations.